Journal of Physics and Chemistry of Solids 111 (2017) 54–62

Contents lists available at ScienceDirect

Journal of Physics and Chemistry of Solids

journal homepage: www.elsevier.com/locate/jpcs

Novel natural super-lattice materials with low thermal conductivity for thermoelectric applications: A first principles study

P.C. Sreeparvathy, V. Kanchana *

Department of Physics, Indian Institute of Technology Hyderabad, Kandi, 502 285, Sangareddy, Telangana, India

ARTICLE INFO

Keywords:
Thermoelectric
Natural super-lattice
Band structure

ABSTRACT

A systematic study which reveals the low thermal conductivity and high thermopower on a series of natural superlattice structures in the form BaXFCh (X: Cu, Ag, Ch: S, Se, Te), LaXSO (X: Cu, Ag) and SrCuTeF are presented. Low thermal conductivity is predicted by combining elastic constants and few well established models. The electronic properties reveal the highly two dimensional nature of band structure in the valence band, and this is confirmed through effective mass calculations. The huge difference in effective mass along different crystallographic directions in valence band introduces anisotropy in the transport properties for hole doping, and 'a' axis is found to be more favourable. In addition to these, the parameter A ($S^2\sigma/\tau T/\kappa_e/\tau$), which can decouple the relaxation time is also calculated, and it reveals the possibility of good thermoelectric properties in these compounds. Our results are comparable with prototype thermoelectric materials, and show better values than traditional TE materials.

1. Introduction

Thermoelectric materials have drawn attention as alternative energy source decades ago, and the wide range of applications and its unique properties made them attractive till today [1]. For commercial applications, the efficiency of the TE materials has to improve, but the conflicting requirements limits the efficiency. The performance of a TE material is defined by the dimensionless figure of merit, zT, given by $zT = \frac{S^2\sigma T}{\kappa}$, where S, σ, κ and T are the thermopower, the electrical conductivity, the thermal conductivity, and the absolute temperature, respectively. κ includes both the electronic κ_e, and the lattice contributions κ_l, i.e, $\kappa = \kappa_e + \kappa_l$. Seebeck coefficient, electrical conductivity and thermal conductivity are the conflicting parameters. Several methods have been adapted to improve the efficiency of a thermoelectric material, and these methods mainly focus on enhancing the power-factor or to suppress the lattice thermal conductivity. Supperlattice is one of the emerging technique which can elevate the efficiency of TE properties by these two methods. The impact of two dimensional quantum well structures on thermoelectric properties have attracted long back itself [2], as there would be more number of controlling parameters to tune the value of zT (figure of merit) compared to normal bulk structures, which means that the thickness also plays a role in these structures. Since the charge carriers in the 2D quantum well structure are confined in a plane (which will be within the plane of layer), the scattering effect along the perpendicular direction will be very less, and that leads to a constant mobility in the plane, whereas the phonons are not confined in any plane, so the interface scattering will be playing a significant role, leading to reduction of lattice thermal conductivity [2]. In addition to this, the thermopower value is also found to be higher in the quasi two dimensional structures. The origin of the large Seebeck coefficient is discussed in the previous study by Kuroki, and they explained that the peculiar band model referred as "pudding-mold" which contain the combination of highly flat and dispersed band [3], could be the reason for high Seebeck coefficient. As we mentioned, superlattice structure can enhance the TE efficiency, but the practical difficulties like lattice mismatch and reproducibility will constrain the production. On this basis, the search for natural superlattice materials which have inherent 2D electronic structure properties are highly demanding. Recent study on Na_xCoO_2 revealed the potential TE property [4], which mainly emerged due to two dimensional electronic structure [5]. Electron doped $FeAs_2$ revealed large Seebeck coefficient due to quasi one dimensional band structure [6]. Layered crystal structures are always interesting to analyse, and the distinct properties of these materials are decided by the bonding within the layers and the bonding between two layers, specifically the weak bonding nature between two layers of the system introduce dimensional reduction. The high temperature superconductivity in La based layered

* Corresponding author.
E-mail address: kanchana@iith.ac.in (V. Kanchana).

http://dx.doi.org/10.1016/j.jpcs.2017.07.009
Received 3 January 2017; Received in revised form 30 June 2017; Accepted 11 July 2017
Available online 14 July 2017

material is an example [7]. Later on, this approach is generalized as new chemistry for zintl-phase compounds, which involves construction of crystal structures out of charge compensating layers, specifically a stable cationic layer, e.g. SrF or LaO, and an anionic functional layer, e.g. FeAs, to make compounds like LaFeAsO [7] or SrFeAsF [8]. The interaction between these two charged layers is Coulombic. The competing charge flow between these two layers makes this zintl-type of compounds more significant for the present research world. The layered crystal structures makes the compounds two-dimensional with quasi-flat electronic structure leading to less dispersive bands at the band edges, resulting in high thermopower in these type of zintl compounds enabling them as good thermoelectric candidates. The hetrolayered '1111′ type compounds have attracted because of several properties, like ionic conductivity, moderate temperature super conductivity and many more [7,9]. The compounds like BiCuSeO [10], SrAgSF [11] have drawn attention to thermoelectricity also. We present further investigation on these series to explore the potential compounds for thermoelectric applications. An ideal thermoelectric material for device application should have, high mechanical strength, high melting point, high Seebeck coefficient, high electrical conductivity and low thermal conductivity. From this point of view we have done an extensive study on this present compounds, which reveals their mechanical, electronic and transport properties. We have chosen zintl-type compounds in the form of BaCuChF (Ch = S, Se, Te), BaAgFCh (Ch = S, Se, Te), SrCuTeF, LaCuSO, LaAgSO for this purpose.

2. Computational details

The electronic band structures were calculated by means of full-potential linear augmented plane wave (FP-LAPW) method based on first-principles density functional theory as implemented in the WIEN2k code [12]. The structural optimisation is carried out to compute the ground state properties within the generalized gradient approximation (GGA) of the Perdew-Burke-Ernzerhof (PBE) potential [13], using the experimental parameters with an energy convergence criterion of 10^{-6} Ry per formula unit. The traditional exchange-correlation potential of Local-Density Approximation (LDA) or Generalized Gradient Approximation (GGA) schemes for the exchange-correlation underestimate the band gaps of semiconductors, and we have used the modified GGA known as the Tran-Blaha modified Becke-Johnson [14] potential (TB-mBJ) [15]. For k-space integrations a $12 \times 12 \times 5$ k-mesh was used. The self-consistent calculations included spin-orbit coupling. The carrier concentration (p for holes and n for electrons) and temperature (T) dependent thermoelectric properties like thermopower (S), electrical conductivity scaled by relaxation time (σ/τ) were calculated using the BOLTZTRAP [16] code, within the Rigid Band Approximation (RBA) [17,18] and the constant scattering time (τ) approximation (CSTA). In the RBA the band structure is assumed unaffected by doping, which only leads to a shift of the chemical potential. For semiconductors it is a good approximation for calculation of the transport properties, when the doping level is not too high [18–23]. In CSTA, the scattering time of electrons is assumed to be independent of the electron energy, while it may depend on carrier concentration and temperature. A detailed discussion of the CSTA is given in Refs. [24–26], and references therein. The only situation where the CSTA can fail is when bipolar conduction is significant, which happens in narrow-gap materials. The phonon dispersion of investigated compounds is calculated using pseudo potential method implemented in Quantum espresso program. Electron localization function (ELF) is calculated using VASP [27].

3. Results and discussions

3.1. Structural properties

The speciality of the investigated compounds originate from the crystal structure itself, where all the compounds crystallize in tetragonal structure with alternative layers of conducting X_2Ch_2 (X: Cu Ag, Ch: S, Se, Te) and insulating Ba_2F_2 segments, see Fig. 1. The structural parameters are optimized using experimental values, and the obtained lattice parameters agree with the experimental values as seen in Table 1. To comment more on structural properties, we have calculated the bond lengths of all the investigated compounds, and are represented in Table 2. It is observed that in BaCuSF, Cu—S bond has more ionic character compared to Ba—F bond, where Cu—S bond length is more close to the sum of the radius of cation and anion, and the same trend is followed for BaCuSeF and BaCuTeF. Among these three compounds, Cu—Te bond in BaCuTeF is found to be more ionic. In the case of BaFAgS, Ag—S bond is found to be more ionic compared to Ba—F bond, and same trend is followed down the column in periodic table. While comparing BaCuSF and BaAgSF, it is observed that all bond length are higher for BaFAgS, and same trend is observed for Se and Te based compounds. In addition to this, Ba—Cu distances in BaCuChF compounds are lesser than Ba—Ag distances in BaAgFS compounds, which might be due to the weak bonding nature of Ag in these compounds, and this is further discussed in the upcoming section. Estimation of bond angle will help to understand the bond distortions, and are represented in Table 2. It is found that in BaCuSF, the bond angle of Ba—F bond is more tetragonally distorted compared to Cu—S bond, where ideal tetragonal bond is 109.5°, and Cu—S bond angle has almost same angle as tetragonal. Bond angles for Ba—F, and X-Ch are found to increase from S to Te, and compared to Cu compounds Ag based compounds have higher bond angle for all the bonds as seen in Table 2. The more distorted bonds may lead to soft lattice and introduce more anharmonicity in lattice thermal conductivity [28]. Now let us analyse the nature of charge density in investigated compounds, and for this we have represented the charge density of [100] plane of BaFAgS (See Fig. 2). From the figure it is evident that along 'xy' plane there is a charge flow, but there is no charge flow along 'z' direction, and this may lead to a huge anisotropy along 'z' direction in the system. For further analysis we have calculated the electron localization function (ELF) for the investigated compounds and in Fig. 3 we have shown the ELF for BaFAgS. ELF can help to identify the chemistry of bonds, and a value close to unity indicate the more covalent character. In Fig. 3 we can see the Ba, S, and F atoms shows this (see the red color), but around Ag atom we found very less ELF value, which indicate the weak Ag bonds in this series. Our results are in line with the previous results for prototype compounds [28].

Moving to electronic structure, we have calculated the band structure using TB-mBJ functional to predict proper band gap of investigated compounds. In Table 1, we have given the band gap using both PBE and TB-mBJ functionals, and from this it is quite clear that the PBE functional underestimate the band gap, and further calculations were performed using TB-mBJ functional only. Fig. 4 represents the band structure of one of the investigated compound, since all the compounds have very similar band structure. The earlier study on these compounds revealed the role of spin-orbit coupling [29], and our calculations also included spin orbit coupling. As we discussed earlier, the investigated compounds crystallize

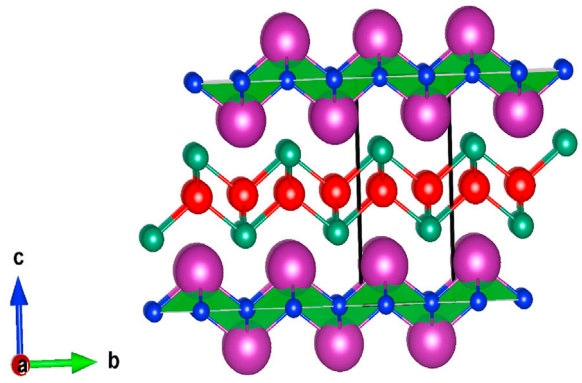

Fig. 1. Crystal structure of investigated compounds.

Table 1
Ground state properties of BaCuChF (Ch = S,Se,Te), SrCuTeF, LaCuSO and LaAgSO with GGA functional along with the available experimental and other calculation results (Space Group: 129 (*P4/nmm*).

	BaCuSF		BaCuSeF		BaCuTeF	
	Present	Exp[a]	Present	Exp[a]	Present	Exp[b]
a(Å)	4.23	4.123	4.25	4.239	4.43	4.4297
c(Å)	9.14	9.0327	9.18	9.1217	9.36	9.3706
Band gap (eV)						
PBE	1.6		1.44		0.99	
TB-mBJ	2.24		2.06		1.52	
	SrCuTeF		LaCuSO		LaAgSO	
	Present	Exp[a]	Present	Exp[a]	Present	Exp[c]
a(Å)	4.27	4.2474	3.87	3.9962	3.92	4.050
c(Å)	9.39	9.2003	8.52	8.5174	8.99	9.039
Band gap (eV)						
GGA	1.18		1.6		1.32	
TB-mBJ	2.06		2.27		2.33	
	BaFAgS		BaFAgSe		BaFAgTe	
	Present	Exp	Present	Exp	Present	Exp
a(Å)	4.33	4.24	4.39	4.34	4.58	–
c(Å)	9.23	9.30	9.57	9.40	9.75	–
Band gap (eV)						
PBE	1.44		1.262		1.56	
TB-mBJ	2.65	–	2.36	–	2.43	–

[a] [36].
[b] [37].
[c] [38].

in the tetragonal structure, the high symmetry $\Gamma - X$ direction indicates the crystallographic $ab-$ plane and $\Gamma - Z$ direction indicates the $c-$ axis of the tetragonal crystal structure. The band gap values are found to decrease down the column in periodic table except for BaFAgTe. All the compounds fall in the range of wide band gap semiconductors. The band structure investigation of this '1111′ type compounds are celebrated because of the highly anisotropic character, and this causes dimensional reduction in these compounds. From the band structure we can see clearly that along the high-symmetry directions $\Gamma - Z$, R-X, M-A, bands are completely flat, which indicate the heavy mass carriers, whereas the dispersive band along $\Gamma - X$ and $\Gamma - A$ indicate the lighter band mass carriers. The inherent nature of the combination of highly flat and dispersed band may lead to the quasi two dimensional structure, which is highly recommended for thermoelectric applications. The prototype compounds have already emerged as good thermoelectric materials [11].

The huge difference in the calculated effective mass confirm the quasi two dimensional nature in the band structure and the values are given in Table 3. For further analysis, we have plotted density of states, which is given in Fig. 5. In the case of BaCuChF compounds Cu-d states are dominating in valence band, whereas in conduction band we can see the mixture of Ba-d and Cu-s states. For SrCuTeF, the Cu states are more dominant in valence band, and Sr and Cu states are prominent in conduction band. For LaCuSO, Cu states are significant in valence band, whereas La states are dominating in the conduction band. For LaAgSO, we can see a strong hybridisation of Ag and S states in valence band, whereas in conduction band La states are dominating. In the case of BaFAgCh, in valence band Ag and Ch states are dominating and in the conduction band we can see the combination of Ba, Ag and Ch states. Overall for all the compounds, the quasi two dimensional bands present in the upper valence band is derived from Cu or Ag 'd' states. Compared to valence band, the states are more hybridised in the conduction band, which may lead to enhanced conduction in electron doping compared to hole doping.

Near valence band we have observed the combination of X and chalcogens, and this may be responsible for the highly two dimensional band character in these investigated compounds, which may lead to high thermopower in these compounds. From the bond analysis, we have observed that Ba—F is tetragonally distorted, which may introduce soft phonons and anharmonicity and cause low thermal conductivity in these compounds.

3.2. Thermoelectric properties

Thermoelectric coefficients like thermopower, electrical conductivity scaled by relaxation are calculated for all the compounds, for the

Table 2
Calculated bond length and bond angle for all the investigated compounds.

	BaCuSF	BaCuFSe	BaCuTeF	BaFAgS	BaFAgSe	BaFAgTe	LaCuOS	LaAgOS	SrCuTeF
A-F(O)(Å)	2.63	2.65	2.65	2.67	2.69	2.72	2.36	2.35	2.53
X-Ch(Å)	2.44	2.55	2.69	2.71	2.79	2.92	2.42	2.51	2.7
F—Ba—F (deg)	67.26	69.07	72.38	69.97	70.43	72.87	73.49	72.06	73.15
Ch-X-Ch(deg)	106.73	107.77	108.89	111.07	112.53	112.8	108.67	113.24	111.93

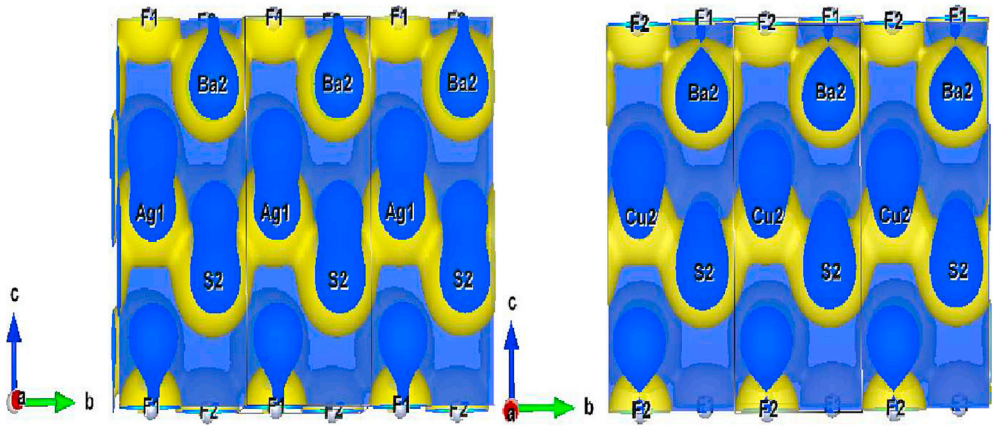

(a) (b)

Fig. 2. (a) Charge density of BaFAgS and BaFCuS along [100] plane. Yellow color surface shows the charge flow. (For interpretation of the references to colour in this figure legend, the reader is referred to the web version of this article.)

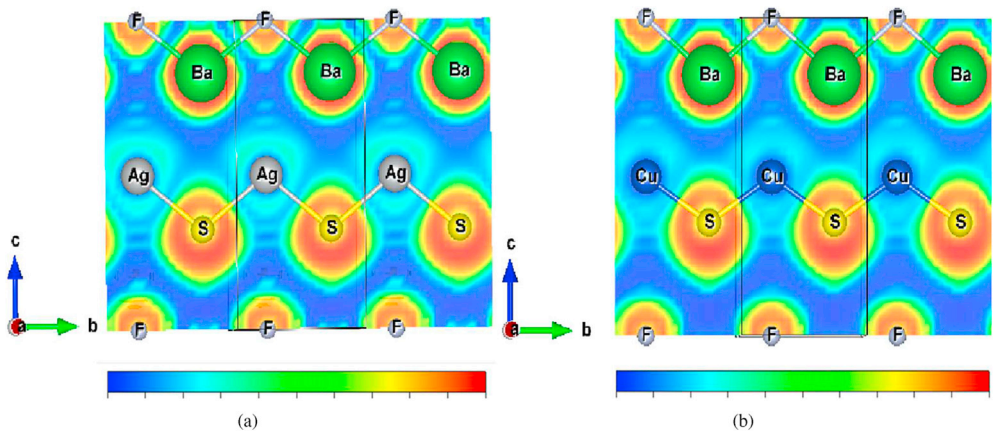

Fig. 3. (a) Electron localization function of BaFAgS and BaCuFS along [100] plane. ELF value high for red and low for blue color in the diagram. (For interpretation of the references to colour in this figure legend, the reader is referred to the web version of this article.)

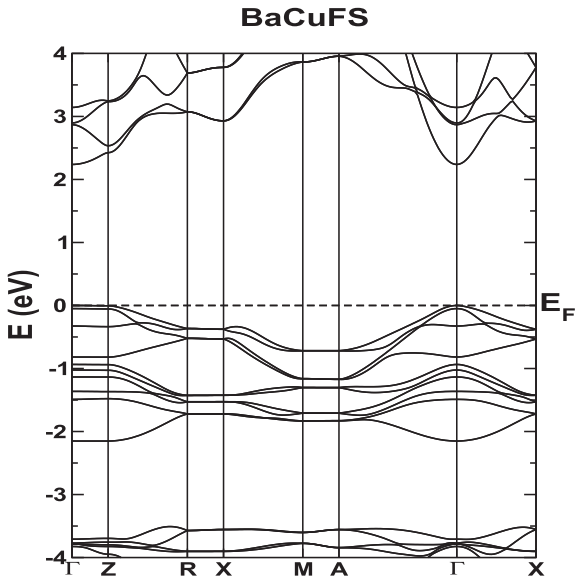

Fig. 4. Calculated band structure for BaCuSF.

Table 3
Calculated effective mass values of BaCuChF (Ch = S, Se, Te) SrCuTeF, LaCuSO and LaAgSO.

Effective mass (me)	BaCuSF		BaCuSeF		BaCuTeF	
	VB	CB	VB	CB	VB	CB
m_z	30.78	1.85	39.61	1.53	32.88	0.96
m_x	5.29	0.68	4.50	0.59	3.48	0.58
Effective mass (me)	SrCuTeF		LaCuSO		LaAgSO	
	VB	CB	VB	CB	VB	CB
m_z	30.78	1.85	39.61	1.53	32.88	0.96
m_x	5.29	0.68	4.50	0.59	3.48	0.58
Effective mass	BaFAgS		BaFAgSe		BaFAgTe	
	VB	CB	VB	CB	VB	CB
m_z	28.91	0.75	21.97	1.10	13.5	1.26
m_x	2.90	1.42	6.02	0.54	3.7	0.64

temperature range 300 K–900 K, and for carrier concentration between $1 \times 10^{18} cm^{-3}$ to $1 \times 10^{21} cm^{-3}$ which is considered as the optimum working range of TE material. The variation of thermopower as a function of carrier concentration for both holes and electrons for different temperatures for BaCuSF is represented in Fig. 6. The magnitude of thermopower is found to decrease with carrier concentration and found to increase with temperature. The nature of thermopower for all the investigated compounds are the same, so we have represented the range of magnitude of thermopower for both holes and electrons for temperatures between 300 K and 900 K as represented in Fig. 7 for all the investigated compounds. Thermopower for hole doping is found to be higher than electron doping for all the cases. Among the investigated compounds, BaCuSF and BaFAgS are found to have maximum value of thermopower. The quasi two dimensional nature in valence band introduce anisotropy in thermopower values for holes along 'a' and 'c' axis.

The electrical conductivity scaled by relaxation time for both the electron and hole concentration is calculated for all the investigated compounds. All the studied compounds have almost similar behaviour and we have represented the variation of electrical conductivity scaled by relaxation time as a function of carrier concentration for the temperature range 300 K–900 K for BaCuSF in Fig. 6. As we expected from the band structure the electrical conductivity for the holes is higher along the 'a' axis compared to the 'c' axis, because the dispersion along the $\Gamma - X$ is more compared to the $\Gamma - Z$. As there is no great difference in the conduction band we can find lesser anisotropy in the case of electrons. We also found the electrical conductivity scaled by relaxation time to be higher in case of electron doping compared to hole doping which is approximately of two orders. The electrical conductivity is found to increase as we move down the group from *S* to *Te* in BaCuChF, which is a regular trend in the periodic table. From the analysis of the thermopower plots of all the compounds, we found that the thermopower is found to increase as we move from S to Se to Te. In contrast to the increase in the thermopower we found a decreasing trend in the electrical conductivity as we move from S to Te in BaCuChF. We also observe an interesting point that the anisotropy is found to be decreasing in both the thermopower and electrical conductivity as we move from S to Te for electron doping. A similar scenario is found in the case of Sr based compounds also. In the case of La-based compounds the anisotropy is found to be lesser in the case of LaCuSO, whereas in LaAgSO significant anisotropy is observed. We can conclude that the investigated compounds can be used for better TE applications.

In order to find the best compound among the investigated series, we plot the power factor $S^2\sigma/\tau$ in Fig. 8. We can see a clear difference among the power factor along 'a' and 'c' directions from this figure. The power factor along the 'a' directions is more dominating than 'c' direction. The position of the peak in this transport function provides an upper bound on the possible optimum doping level, and this is below $\sim 10^{21} cm^3$ holes for all investigated compounds. Among the investigated compounds the power factor of BaCuSeF is found to be higher for the hole doping. The present studied compounds have comparable value of thermopower and

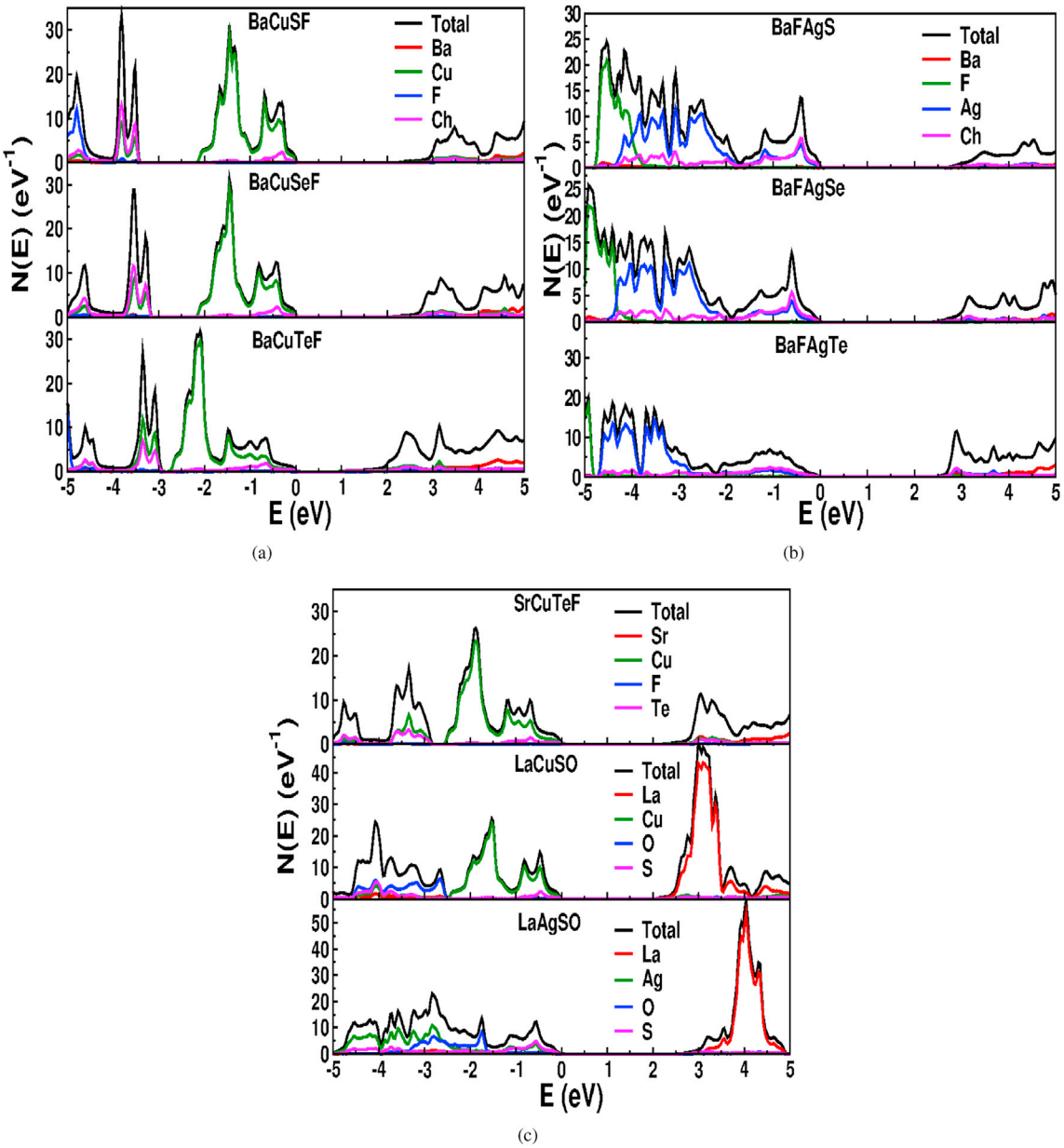

Fig. 5. Calculated density of states of all the investigated compounds.

electrical conductivity scaled by relaxation time as that of the prototype compound SrAgSF [11], which is realised as a natural superlattice.

We know that the figure of merit depends on thermopower, electrical conductivity, thermal conductivity and absolute temperature. In our present calculations the value of electrical conductivity is coupled with the relaxation time. Now let us examine the decoupling of relaxation time and to comment more about the figure of merit. For this purpose we are following the method proposed by Takeuchi [30] to decompose zT in two parts 'A' and 'B', where 'A' is purely dependent on electronic part and 'B' contains the lattice thermal conductivity part.

$$zT = \left(S^2\sigma T/k_e + k_l\right) = AB, \quad A = \left(S^2\sigma T/k_e\right),$$

$$B = 1/(1 + k_l + k_e)$$

Since the value of 'B' is less than unity, 'A' can be considered as the maximum possible value of zT. The parameter 'A' is defined as $(S^2\sigma T/\kappa_e)$. In our case both electrical conductivity and electronic part of thermal conductivity are coupled with relaxation time, and by using this formula we can decouple it. The range of 'A' parameter for investigated compounds are given in Fig. 9. Since both electrical conductivity scaled by relaxation time and electronic part of thermal conductivity scaled by relaxation time have anisotropy along 'a' and 'c' axis, there is no much anisotropy observed in 'A' parameter.

Since the thermopower and electrical conductivity values are good enough within the studied temperature range 300 K–900 K, the investigated compounds find promising TE applications for a wide temperature range.

3.3. Lattice dynamics

Understanding the mechanical stability and elastic properties of materials are important for device applications, and the present section deals with these two properties. We start with the analysis of six elastic constants of the investigated compounds, and calculated elastic constants are given in Table 4, which satisfy the Born criteria [32] for stability. To understand the stiffness along different crystallographic directions, we have compared the elastic constants along these directions. As we know

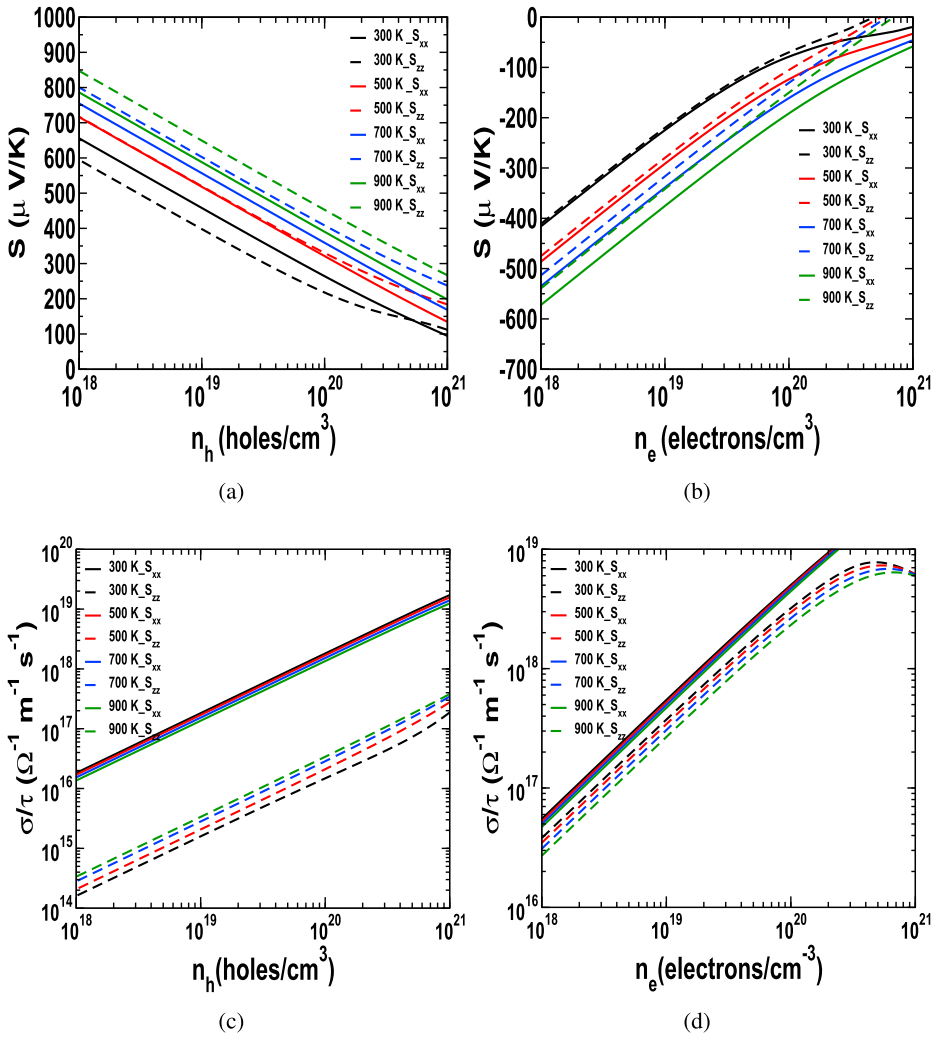

Fig. 6. Calculated thermopower for (a) electrons and (b) holes; electrical conductivity scaled by relaxation time for (c) electrons and (d) holes of BaCuSF.

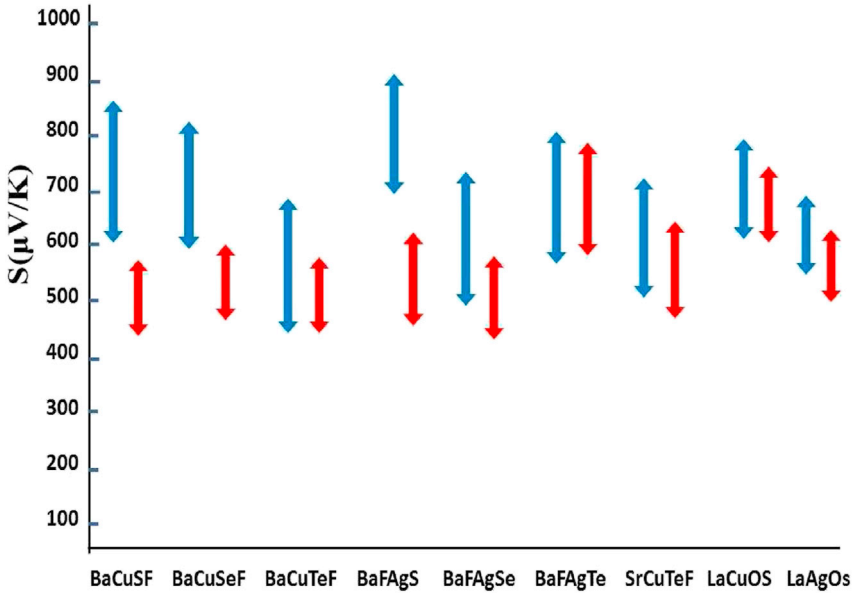

Fig. 7. Calculated thermopower values of all the investigated compounds for temperature range 300 K–900 K, and carrier concentration 1×10^{18} to 1×10^{21}.

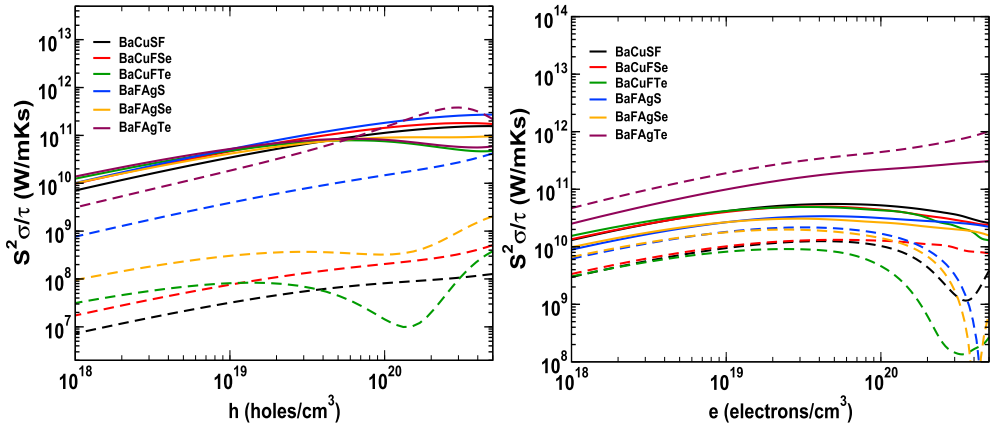

Fig. 8. Calculated power factor of all the investigated compounds.

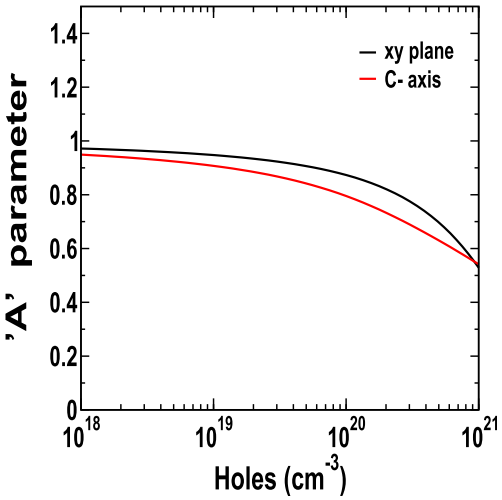

Fig. 9. Calculated 'A' parameter of BaCuSF.

Table 4
Calculated elastic constants of BaCuChF (Ch = S, Se, Te) SrCuTeF, LaCuSO and LaAgSO.

Parameters	BaCuSF	BaCuSeF	BaCuTeF	SrCuTeF	LaCuSO	LaAgSO
C_{11} (GPa)	106.20	98.91	88.20	94.45	216.58	215.51
C_{33} (GPa)	98.40	99.91	53.05	60.69	104.61	101.08
C_{44} (GPa)	34.73	33.52	29.54	27.48	44.56	35.94
C_{66} (GPa)	17.94	17.75	17.27	18.40	57.04	64.21
C_{12} (GPa)	27.94	25.26	15.60	17.61	80.71	57.12
C_{13} (GPa)	45.73	42.22	29.76	32.68	66.04	57.18
Bulk Modulus(B) (GPa)	60.50	41.11	43.7	45.42	92.34	85.42
V_l (km/s)	4.28	3.99	3.43	3.74	5.05	4.76
V_t (km/s)	2.31	2.14	1.96	1.92	2.57	2.47
V_m (km/s)	2.58	2.39	2.18	2.15	2.88	2.74
θ_D (K)	286.67	260.57	228.03	230.80	341.48	315.41
k_{min} (W/mK)	0.43	0.38	0.29	–	0.51	

Parameters	BaFAgS	BaFAgSe	BaFAgTe
C_{11} (GPa)	97.39	96.36	82.71
C_{33} (GPa)	73.76	57.36	63.15
C_{44} (GPa)	27.64	26.03	15.00
C_{66} (GPa)	14.97	15.70	11.32
C_{12} (GPa)	32.31	28.98	31.31
C_{13} (GPa)	46.90	37.67	42.17
Bulk Modulus(B) (GPa)	57.50	50.97	51.01
V_l (km/s)	3.92	3.58	3.34
V_t (km/s)	1.98	1.88	1.54
V_m (km/s)	2.22	2.11	1.74
θ_D (K)	237.39	220.894	175.40
k_{min} (W/mK)	0.36	0.32	0.26

for the tetragonal system C_{11} and C_{22} will be same (along 'a' and 'b' axis) and C_{33} is along 'c' axis, and it is observed that C_{11} is higher than C_{33}, which indicates that 'a' axis is more stronger than c axis, which again is obvious from the bonding itself, as the distance between Ba-Ch is higher compared to other bond lengths in the system, and this may lead to easy compression along 'c' axis. Further we observed that magnitude of elastic constants of Ag based compounds are lesser than Cu based compounds, and this indicate the weak Ag bonding in these compounds, and the same we have mentioned in ELF calculations also. In addition, the large shear constants (C_{11}—$C_{12}/2$) in Cu based compounds indicate the higher mechanical strength in this. The magnitude of C_{12} is further related with the bonding in 'x' and 'y' plane, so the large value of C_{12} in Cu based compounds indicate the stronger bond in 'x' and 'y' plane of this series compared to Ag based compounds, which was also obvious from the bond length calculations, where we have observed the higher bond length for Ag based compounds compared to Cu based compounds. From elastic constants, we have further calculated other mechanical properties like bulk moduls, shear modules etc, and are represented in Table 4. All compounds fall in the region of ductile materials. Bulk modulus is found to decrease from S to Te in both Cu and Ag based compounds, and is observed that the range of bulk modulus is comparable with well known prototype materials BiOCuSe [28], and SrAgChF [11]. Further the anisotropy in bulk modulus, which is defined as Ba/Bc = (C_{11}—C_{13})+(C_{12}—C_{13})/(C_{33}—C_{13}) is also analysed and is found that for Ag based compounds there is an anisotropy between 'a' and 'c' axes. We also found that the oxygen based chalcogen have higher bulk modulus values compared to the fluro based chalcogens (see Table 4). Longitudinal and transverse sound velocities are calculated and observed that for all the compounds there is an anisotropy in these compounds. Further, calculated Debye temperature (see Table 4) indicate the possibility of very low thermal conductivity in these investigated compounds, and have almost comparable values with prototype materials. The Grünesian parameter relates the phonon frequencies and crystal volume, and by calculating this we can comment about the rate of anharmonicity in phonon conduction. Here we have calculated the average Grünesian parameter of investigated compounds are given in Table 5, and from table it is clear that the investigated compounds have Grünesian parameter lesser than prototype material BiOCuSe, and other TE material SnSe [33], which indicate the lesser anharmonicity in phonon conduction. In this scenario, the prediction of lattice thermal conductivity from calculated Debye temperature and Grünesian parameter is worthy. One of the pioneering work regarding thermal conductivity by G. A. Slack [34]has been adapted here to predict the thermal conductivity of investigated compounds. The main assumption used here is that the heat is only conducted by acoustic phonons. The Slack's equation for thermal conductivity is

$$k = 3.1 \times 10^{-6}\left(M\theta^3\delta/\gamma^2 n^{2/3}T\right) \text{ in } Wm^{-1}k^{-1}$$

Table 5
Calculated Grünesian parameter and lattice thermal conductivity at 300 K of all compounds.

Parameters	BaFAgS	BaFAgSe	BaFAgTe	BaCuSF	BaCuSeF	BaFCuTe	LaCuOS	LaOAgS	SrCuTeF
γ	1.97	1.82	2.26	1.74	1.73	1.53	1.94	1.87	1.91
k (W m^{-1} K^{-1})	1.84	2.05	0.79	3.46	3.27	3.23	4.31	4.4	1.79

where M is average atomic mass in amu, θ is Debye temperature in K, δ^3 is Volume per atom in Å^3, 'n' is number of atoms in the primitive cell, γ is average Grünesian parameter. Since the contribution of optical modes of phonons towards thermal conductivity is lower compared to acoustic phonons, this equation is worthy to be used for predicting the range of the thermal conductivity. Calculated values of thermal conductivity of investigated compounds using Slack's equation are given in Table 5. From the table, it is quite clear that all the compounds possess very low thermal conductivity. The exact value of thermal conductivity may differ from the calculated values little bit because of the exclusion of anharmonic effects, which has be to verified further by future studies. The low value of Debye temperature confirms the higher atomic mass and weak inter atomic bonding, while the range of Grünesian parameter indicate the moderate anharmonicity in these compounds [34]. This confirms that the investigated compounds can emerge as good thermoelectric materials which can be realised with future experimental studies. For further proof we have used Cahill model [35] to find the range of minimum thermal conductivity in studied compounds. According to Cahill model, the equation of minimum thermal conductivity is

$$k_{\min} = \mathrm{k}_B/2.48\left(\mathrm{n}^{2/3}(v_l + 2v_t)\right)$$

where k_B is the Boltzmann constant, n is the density of number of atoms per volume, v_l and v_t are average longitudinal and transverse velocities. Calculated values of k_{min} are given in Table 4. Further we have also related the anisotropy in lattice thermal conductivity values by using Young's modulus. Since lattice thermal conductivity is proportional to v^3, and v is proportional to Y (Yong's modulus). We have estimated the anisotropy in lattice thermal conductivity in a crude way by comparing with Young's modulus along different axis.

$$\mathrm{Y}_c = \mathrm{C}_{33} - (2\mathrm{C}_{13}2\mathrm{C}_{13}/\mathrm{c}_{11} + \mathrm{c}_{12})$$

$$\mathrm{Y}_a = ((\mathrm{C}_{11} - \mathrm{C}_{12})(\mathrm{C}_{11}\mathrm{C}_{13} + \mathrm{C}_{12}\mathrm{C}_{33} - 2\mathrm{C}_{13}\mathrm{C}_{13}))/(\mathrm{C}_{11}\mathrm{C}_{33} - \mathrm{C}_{13}\mathrm{C}_{13})$$

From our calculations it is observed that lattice thermal conductivity also possess anisotropy along different crystallographic direction and found to be more along 'a' axis than 'c' axis.

For further analysis we have calculated the phonon dispersion of the investigated compounds. The phonon dispersion relation of few of the compounds, and phonon density of states of BaFAgS are presented in Fig. 10 to understand the behaviour of phonon modes, and the dynamical stability of the investigated compounds. The positive values of frequencies confirmed the dynamical stability of the investigated compounds. To understand about the thermal conductivity, we have to examine the interaction between acoustic and optical modes of the dispersion plots. We have observed that the optic branches intersect the acoustic branches around 44 cm^{-1} for SrCuTeF, around 60 cm^{-1} for BaFAgS, around 40 cm^{-1} for BaFAgTe, around 54 cm^{-1} for LaAgOS and around 81 cm^{-1} for LaCuOS. To understand which states are contributing near low frequency range, we have investigated the phonon density of states of BaFAgS, and are represented in the same figure. From the figure it is clear that Ag and S states are dominating at low frequency range. The trend indicate that for all investigated compounds the interaction between low frequency optical modes and acoustic modes are high. We know that to reduce the lattice thermal conductivity we need higher phonon scattering, which is obvious from the phonon plots. Further we can see the flat acoustic branches, which again indicate the low thermal conductivity in these compounds. Here we would like to recall the

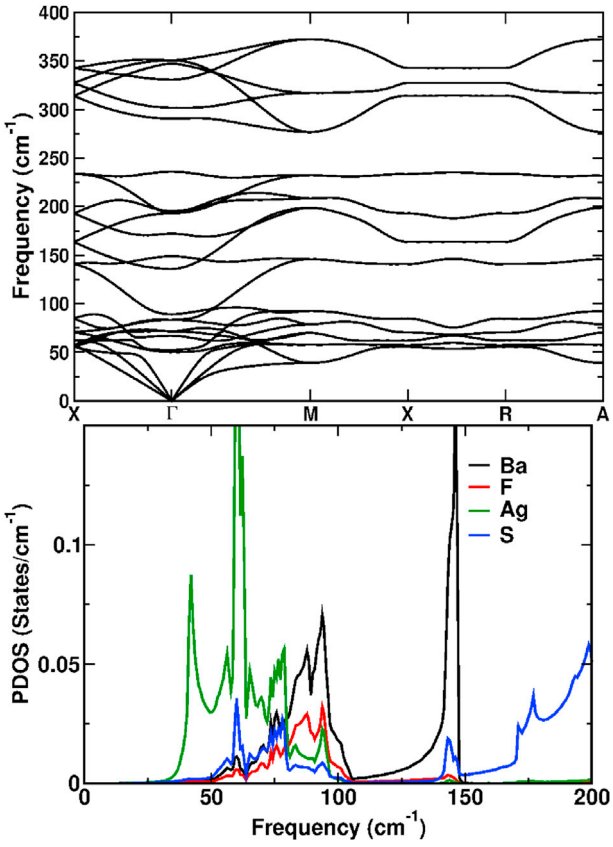

Fig. 10. Calculated phonon dispersion and phonon density of sates of BaFAgS.

bonding and electronic structure analysis, where we have noticed that the highly quasi flat band nature was derived from the X-Ch states, and from the phonon density of states it is quite clear that low frequency phonon modes are derived from X-Ch states, and this again emphasises the role of natural super lattice structure in thermoelectrics. The remarkable structure of these family of compounds showed a combination of high thermopower and low thermal conductivity, and further the electrical conductivity can be enhance by doping calculations, which eventually project this series to be promising thermoelectric materials. All the calculations are in line and showed that all the investigated compounds have very low thermal conductivity.

4. Conclusions

The electronic, mechanical and transport properties of BaXChF (X: Cu, Ag, Ch: S, Se, Te), LaXOS and SrCuTuF were calculated using density functional theory. The analytical calculations revealed the low thermal conductivity in these compounds. The quasi two dimensional nature of band structure is identified, and all the investigated compounds can be considered as natural super-lattice structures. The calculated thermopoer values are found to be higher for all the compounds. Huge anisotropy is observed for electrical conductivity scaled by relaxation time for hole doping, which confirms again the quasi two dimensional nature in these compounds. The transport properties of all the investigated compounds are comparable with the prototype material SrAgSF. The low value of

Debye temperature and highly interacting acoustic and optical phonon modes confirm the possibility of low thermal conductivity in these compounds. The calculated 'A' parameter have higher values than traditional TE materials. The merge of high power factor and low thermal conductivity can site these compounds for better TE applications.

Acknowledgement

The authors SPC and VK would like to thank IIT Hyderabad for computational facility, and SP would like to thank MHRD for fellowship, Vijay Kumar Gudelli for timely support.

References

[1] Gangjian Tan, Li-Dong Zhao, Mercouri G. Kanatzidis, Chem. Rev. 116 (19) (2016) 12123–12149.
[2] L.D. Hicks, M.S. Dresselhaus, Phys. Rev. B 47 (1993) 12727.
[3] K. Kuroki, R. Arita, J. Phys. Soc. Jpn. 76 (2007) 083707.
[4] I. Terasaki, Y. Sasago, K. Uchinokura, Phys. Rev. B 56 (1997) 12685.
[5] D.J. Singh, Phys. Rev. B 61 (2000) 13397.
[6] Hidetomo Usui, Kazuhiko Kuroki, Seiya Nakano, Kazutaka Kudo, Minoru Nohara, Phys. Rev. B 88 (2013) 075140.
[7] Y. Kamihara, T. Watanabe, M. Hirano, H. Hosono, J. Am. Chem. Soc. 130 (2008) 3296.
[8] F. Han, X. Zhu, G. Mu, P. Cheng, H.H. Wen, Phys. Rev. B 78 (2008) 180503.
[9] M. Palazzi, S. Jaulmes, Structure du conducteur ionique (LaO)AgS, Acta Crystallogr. B 37 (1981) 1337–1339.
[10] S.K. Saha, Phys. Rev. B 92 (2015), 041202(R).
[11] V.K. Gudelli, V. Kanchana, G. Vaitheeswaran, David J. Singh, A. Svane, N.E. Christensen, S.D. Mahanti, Phys. Rev. B 92 (2015) 045206.
[12] P. Blaha, K. Schwarz, G.K.H. Madsen, D. Kvasnicka, J. Luitz, WIEN2K, an Augmented Plane Wave + Local Orbitals Program for Calculating Crystal Properties, Karlheinz Schwarz, Techn. Universität Wien, Austria, 2001.
[13] J.P. Perdew, K. Burke, M. Ernzerhof, Phys. Rev. Lett. 77 (1996) 3865–3868.
[14] A.D. Becke, E.R. Johnson, J. Chem. Phys. 124 (2006) 221101.
[15] F. Tran, P. Blaha, Phys. Rev. Lett. 102 (2009) 226401.
[16] G.K.H. Madsen, D.J. Singh, Comput. Phys. Commun. 175 (2006) 67–71.
[17] T.J. Scheidemantel, C. Ambrosch-Draxl, T. Thonhauser, J.V. Badding, J.O. Sofo, Phys. Rev. B 68 (2003) 125210.
[18] L. Jodin, J. Tobola, P. Pecheur, H. Scherrer, S. Kaprzyk, Phys. Rev. B 70 (2004) 184207.
[19] L. Chaput, P. Pecheur, J. Tobola, H. Scherrer, Phys. Rev. B 72 (2005) 085126.
[20] D.I. Bilc, S.D. Mahanti, M.G. Kanatzidis, Phys. Rev. B 74 (2006) 125202.
[21] J.M. Ziman, Electrons and Phonons: Theory of Transport Phenomena in Solids, Oxford University Press, London, UK, 1960.
[22] B.R. Nag, Electron Transport in Compound Semiconductors, Springer-Verlag, Berlin, 1980.
[23] D.J. Singh, I.I. Mazin, Phys. Rev. B 56 (1997) R1650.
[24] D.J. Singh, Funct. Mat. Lett. 3 (2010) 223–226.
[25] D. Parker, D.J. Singh, Phys. Rev. B 85 (2012) 125209.
[26] K.P. Ong, D.J. Singh, P. Wu, Phys. Rev. B 83 (2011) 115110.
[27] G. Kresse, J. Hafner, Phys. Rev. B 47 (1993) 558.
[28] S.K. Saha, G. Dutta, Phys. Rev. B 94 (2016) 125209.
[29] A. Zakutayev, R. Kykyneshi, G. Schneider, D.H. McIntyre, J. Tate, Phys. Rev. B 81 (2010) 155103.
[30] T. Takeuchi, Mater. Trans. 50 (2009) 2359.
[32] R. Hill, The elastic behaviour of a crystalline aggregate, Proc. Phys. Soc. Sect. A 65 (1952) 349354.
[33] Li-Dong Zhao, Shih-Han Lo, Yongsheng Zhang, Hui Sun, Gangjian Tan, Ctirad Uher, C. Wolverton, Vinayak P. Dravid, Mercouri G. Kanatzidis, Nature 508 (2014) 373377.
[34] G.A. Slack, J. Phys. Chem. Solids 34 (1973) 321–335.
[35] D.G. Cahill, S.K. Watson, R.O. Pohl, Phys. Rev. B 46 (1992) 6131.
[36] Hiroshi Yanagi, Janet Tate, Sangmoon Park, Cheol-Hee Park, Douglas A. Keszler, Masahiro Hirano, Hideo Hosono, J. Appl. Phys. 100 (2006) 083705.
[37] Cheol-Hee Park, Robert Kykyneshi, Alexandre Yokochi, Janet Tate, Douglas A. Keszler, J. Solid State Chem. 180 (2007) 1672–1677.
[38] P.M. Palazzi, S. Jaulmes, Acta Cryst. B37 (1981) 1337–1339.